

HOKKAIDO UNIVERSITY

Title	Central-Obscuration Removal Plates for Focal-Plane Phase-Mask Coronagraphs with a Centrally-Obscured Telescope
Author(s)	Oshiyama, Fumika; Murakami, Naoshi; Guyon, Olivier et al.
Citation	Publications of the Astronomical Society of the Pacific, 126(937), 270-279 https://doi.org/10.1086/675807
Issue Date	2014-03-01
Doc URL	https://hdl.handle.net/2115/58041
Type	journal article
File Information	Oshiyama_2014_PASP_126_270.pdf



Hokkaido University Collection of Scholarly and Academic Papers : HUSCAP

PUBLICATIONS OF THE ASTRONOMICAL SOCIETY OF THE PACIFIC, **126**:270–279, 2014 March
© 2014. The Astronomical Society of the Pacific. All rights reserved. Printed in U.S.A.

Central-Obscuration Removal Plates for Focal-Plane Phase-Mask Coronagraphs with a Centrally-Obscured Telescope

FUMIKA OSHIYAMA,[1] NAOSHI MURAKAMI,[2,3] OLIVIER GUYON,[4] FRANTZ MARTINACHE,[5] NAOSHI BABA,[2] TARO MATSUO,[6] JUN NISHIKAWA,[7,8] AND MOTOHIDE TAMURA[7,9]

Received 2013 December 06; accepted 2014 January 31; published 2014 March 7

ABSTRACT. Focal-plane phase-mask coronagraphs, such as eight-octant phase-mask coronagraphs (8OPM), are one of the most promising tools for high contrast observations. However, coronagraphic performance would be degraded when combined with a centrally-obscured telescope. We propose pupil-remapping optics for removing the shade of a secondary mirror to generate a clear, circular pupil for the phase-mask coronagraph. First, we show the design of the pupil-remapping optics, called central-obscuration removal plates (CRPs). Next, we report laboratory experiments on the 8OPM coronagraph using manufactured CRPs. We also evaluate off-axis point-spread functions via both laboratory experiments and numerical simulations. Finally, we evaluate, via numerical simulations, limiting factors for coronagraphic performance, such as phase aberrations introduced by the CRPs, the effect of Fresnel diffraction, and chromatic behavior. The numerical simulations suggest that the phase aberrations could be a dominant limiting factor of the achievable contrast in the current laboratory experiments.

Online material: color figures

1. INTRODUCTION

Recent progress in techniques for astronomical observations is remarkable, and now more than 1000 extrasolar planets have been discovered, mainly by indirect detection methods like radial velocity and transit methods. Furthermore, several large extrasolar planets have been directly detected (Kalas et al. 2008; Marois et al. 2008; Lagrange et al. 2009; Thalmann et al. 2009; Kuzuhara et al. 2013). These extrasolar planets have been observed mainly by a classical Lyot coronagraph and an angular differential imaging technique.

Development of observational technology in the near future will enable direct detection of lower-mass planets closer to their host stars. New ground-based high-contrast imaging instruments, such as SCExAO/Subaru, GPI/Gemini, and SPHERE/VLT, have started operating (Macintosh et al. 2008; Beuzit et al. 2008; Martinache & Guyon 2009). For these instruments, advanced coronagraphs such as the apodized pupil Lyot coronagraph (APLC) and the phase-induced amplitude apodization (PIAA) have been developed (Soummer et al. 2003; Guyon 2003). A four-quadrant phase-mask coronagraph, one kind of focal-plane phase-mask coronagraph, has also been developped for the SPHERE/VLT (Mawet et al. 2006; Boccaletti et al. 2008).

The phase-mask coronagraphs are attractive methods, which realize good detectability with a relatively simple optical system. Several extrasolar planets, such as HR8799 b,c,d, and β Pictoris b, have been directly imaged by use of the phase-mask coronagraphs (Serabyn et al. 2010; Absil et al. 2013). The phase-mask coronagraph can theoretically realize perfect elimination of light from a point-like star when it is combined with a clear circular telescope pupil. However, the star light cannot be eliminated perfectly when using a conventional telescope pupil that has a central obscuration due to a secondary mirror. To solve this problem, observations with a circular subaperture extracted from the 200-inch telescope of Palomar Observatory was reported (Serabyn et al. 2009; Mawet et al. 2009, 2010; Serabyn et al. 2010). In addition, several techniques have been proposed for reducing the effect of the central obscuration (Abe et al. 2006; Mawet et al. 2011, 2013).

In this paper, we propose a method to remove the central obscuration using two specially designed plates. By using these compensating plates, the phase-mask coronagraph can

[1] Division of Applied Physics, Graduate School of Engineering, Hokkaido University, Sapporo, Hokkaido, 060-8628, Japan.
[2] Division of Applied Physics, Faculty of Engineering, Hokkaido University, Sapporo, Hokkaido, 060-8628, Japan.
[3] Jet Propulsion Laboratory, California Institute of Technology, 4800 Oak Grove Drive, Pasadena, CA, 91109 nmurakami@eng.hokudai.ac.jp.
[4] Subaru Telescope, 650 N. A'ohoku Place, HI, 96720.
[5] Observatoire de la Cote d'Azur, Laboratoire Lagrange, CNRS UMR 7293, Boulevard de l'Observatoire, Nice, 06304, France.
[6] Graduate Shool of Science, Kyoto University, Kyoto, 606-8502, Japan.
[7] Division of Optical and Infrared Astronomy, National Astronomical Observatory of Japan, Mitaka, Tokyo, 181-8588, Japan.
[8] School of Physical Sciences, Graduate University for Advanced Studies, Mitaka, Tokyo, 181-8588, Japan.
[9] Department of Astronomy, The University of Tokyo, 7-3-1, Hongo, Bunkyo-ku, Tokyo, 113-0033, Japan.

be installed into a centrally-obscured telescope without loss of incoming photons and without degradation of angular resolution. The principle of the phase-mask coronagraph is described in § 2 in the context of degradation of coronagraphic performance due to central obscuration. Design of the compensating plates is shown in § 3. In § 4, we show results of laboratory experiments for demonstrating the removal of the central obscuration using the manufactured plates. We also show experimental results of the phase-mask coronagraph combined with the compensating plates. In addition, numerically simulated and experimentally obtained off-axis point-spread functions (PSFs) are also shown in § 4 to evaluate the off-axis performance. In § 5, we investigate, by means of numerical simulations, effects of phase aberrations of the compensating plates and Fresnel diffraction on the coronagraphic performance. We also mention chromatic behavior due to these effects. Finally, we summarize our conclusion in § 6.

2. PHASE-MASK CORONAGRAPH WITH CENTRALLY-OBSCURED TELESCOPE PUPIL

Many kinds of focal-plane phase masks have been proposed to date, such as four-quadrant phase mask (4QPM), eight-octant phase mask (8OPM), and optical or vector vortex masks (Rouan et al. 2000; Murakami et al. 2008; Foo et al. 2005; Mawet et al. 2005). These phase masks will realize perfect stellar elimination, assuming that a telescope pupil does not have a central obscuration. The clear circular telescope pupil can be obtained by an off-axis telescope or a subaperture extracted from a conventional telescope pupil.

Figure 1 shows an optical setup of the 8OPM coronagraph. A complex amplitude on a telescope focal plane $E_{f1}(\rho, \phi)$ is connected with that on an entrance pupil plane $E_{p1}(r, \theta)$ by Fourier transform. When a circular telescope pupil with a diameter D is expressed as $E_{p1}(r, \theta) = \Pi_D(r, \theta)$, the complex amplitude on the focal plane after passing through a phase mask is written as

$$E_{f1}(\rho, \phi) = \mathcal{F}[\Pi_D(r, \theta)]M(\rho, \phi), \tag{1}$$

where $M(\rho, \phi)$ is an amplitude transmittance of the phase mask, and $\mathcal{F}$ is the Fourier-transform operator. Therefore, an amplitude on a relayed pupil plane will be written by using the inverse-Fourier-transform operator $\mathcal{F}^{-1}$ and the convolution operator $*$ as

$$E_{p2}(r, \theta) = \Pi_D(r, \theta) * \mathcal{F}^{-1}[M(\rho, \phi)]. \tag{2}$$

The phase masks theoretically generate a zero-amplitude, $E_{p2}(r, \theta) = 0$, over the telescope pupil area, and star light from an on-axis direction is totally diffracted outside the pupil area. Thus the on-axis star light is perfectly blocked by a Lyot stop, and light from off-axis directions, such as planetary light, can be received by a detector.

When the telescope pupil has a central obscuration with a diameter of aD, $E_{p1}(r, \theta)$ is written as $\Pi_D(r, \theta)$–$\Pi_{aD}(r, \theta)$. In this case, $E_{p2}(r, \theta)$ will be written as

$$E_{p2}(r, \theta) = \Pi_D(r, \theta) * \mathcal{F}^{-1}[M(\rho, \phi)] - \Pi_{aD}(r, \theta) * \mathcal{F}^{-1}[M(\rho, \phi)]. \tag{3}$$

The first term is identical to that of equation (2), while the second term is a downsized copy of the first term mainly distributed inside the pupil area.

Numerically simulated images on the relayed pupil plane $|E_{p2}(r, \theta)|^2$, without and with a secondary mirror, are shown in Figure 2. When a telescope pupil has the central obscuration, star light cannot be perfectly blocked by the Lyot stop, because residual light appears inside the pupil area. Thus, the intensity of

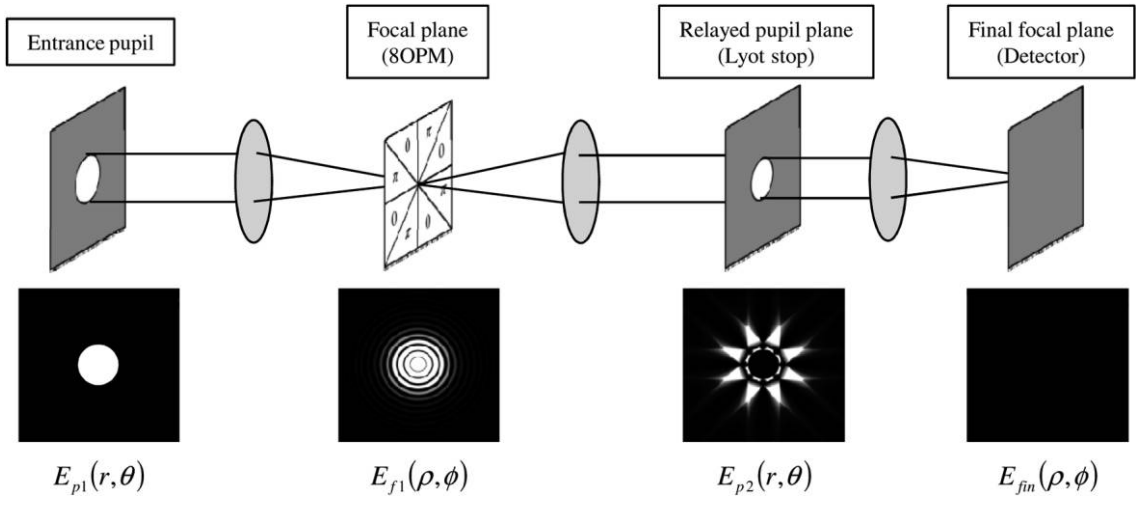


FIG. 1.—An optical setup of an eight-octant phase-mask coronagraph.

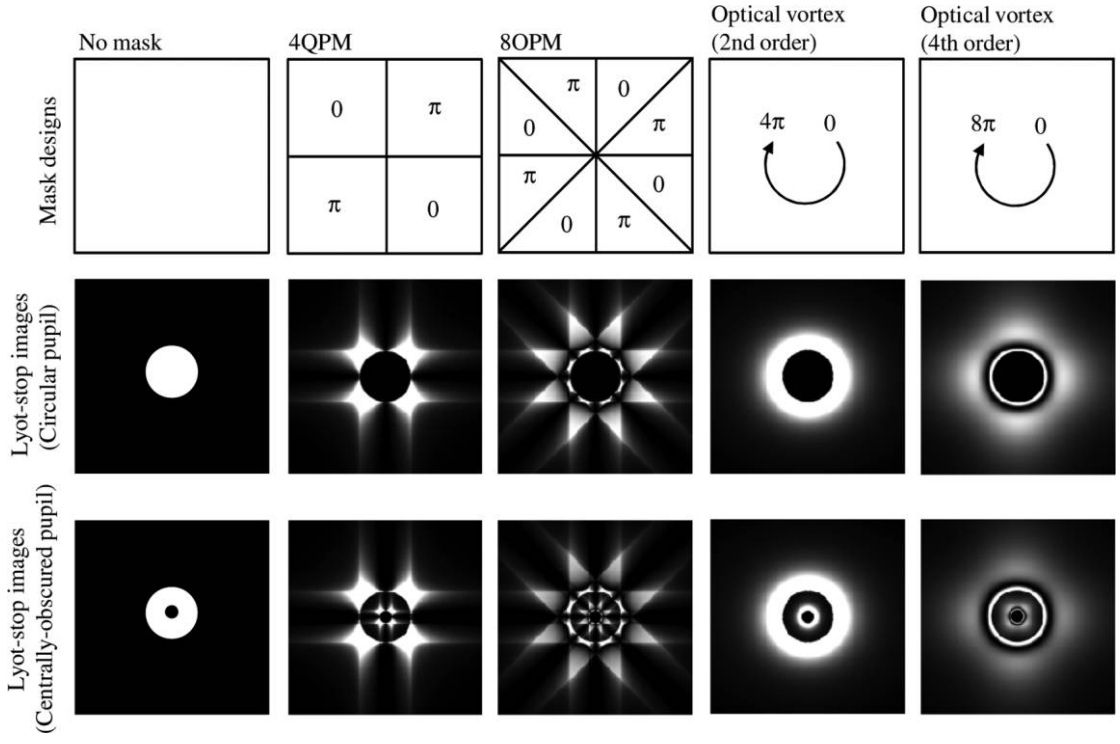


FIG. 2.—Numerical simulations of phase-mask coronagraphs without and with a central obscuration.

a coronagraphic final image, $|E_{\rm fin}(\rho,\phi)|^2$, does not become 0 when the centrally-obscured telescope pupil is used. Thus, the effect of the central obscuration should be reduced to enhance the coronagraphic performance.

3. CENTRAL-OBSCURATION REMOVAL PLATES

3.1. Design of Optical-Surface Shapes

To install the phase-mask coronagraphs into a conventional telescope, it would be necessary to remove the central obscuration. Compensating pupil-remapping mirrors and axicon-like lenses have been proposed to remove the central obscuration (Murakami & Baba 2005; Murakami et al. 2010a). We note that, however, these optics will require additional apodizers to flatten a beam profile. Here, we propose a new design of pupil-remapping optics, central-obscuration removal plates (CRPs), for directly transforming the beam profile from a centrally-obscured telescope pupil to a clear circular one.

Figure 3 shows an optical configuration of the phase-mask coronagraph for a centrally-obscured telescope. Besides the secondary mirror, the conventional telescope pupil also has the obscuration due to the supporting structure, i.e., spider vanes. The CRPs cannot remove the shade of the spider vanes. The residual spider pattern would degrade the coronagraphic performance. Our preliminary numerical simulations suggest that the residual spider pattern would limit the contrast to $\sim 10^{-6}$ at $\sim 7\,\lambda/D$. The problem of the residual spider has to be resolved before achieving higher contrast. However, it will be difficult to design and manufacture remapping devices to remove both central obscuration and spider pattern simultaneously. Several techniques have been proposed for removing the spider pattern, such as the spider removal plate (SRP) or active correction of aperture discontinuities (ACAD) (Lozi et al. 2009; Pueyo & Norman 2013).

Similar to the PIAA, the CRPs also distort phase of off-axis wavefront. Thus, the quality of the off-axis PSF deteriorates as the angular separation of the off-axis light beam becomes larger. As a result, an effective field of view (FOV) of the phase-mask coronagraph would be limited. To recover the quality of the off-axis PSF and improve the FOV, it is necessary to place the reverse correcting optics (inverse CRPs, ICRPs) behind the Lyot stop.

We designed the CRPs based on a coordinate system shown in Figure 4 (Galicher et al. 2005). We assume that two plates are made of dielectric material with a refractive index n. In addition, we assume that a front side of the first plate and a rear side of the second plate are flat surfaces. When a light beam propagates in parallel with the z-axis with a distance $r = r_1$, this beam enters the first plate at a position $(r_1, z_1(r_1))$ and refracts, then enters the second plate at a position $(r_2, z_2(r_2))$. The light beam refracts again at the front side of the second plate, and emits from the second plate in parallel with the z-axis.

By applying the Snell's law, the following two differential equations can be derived for describing optical surfaces of the CRPs (Galicher et al. 2005):

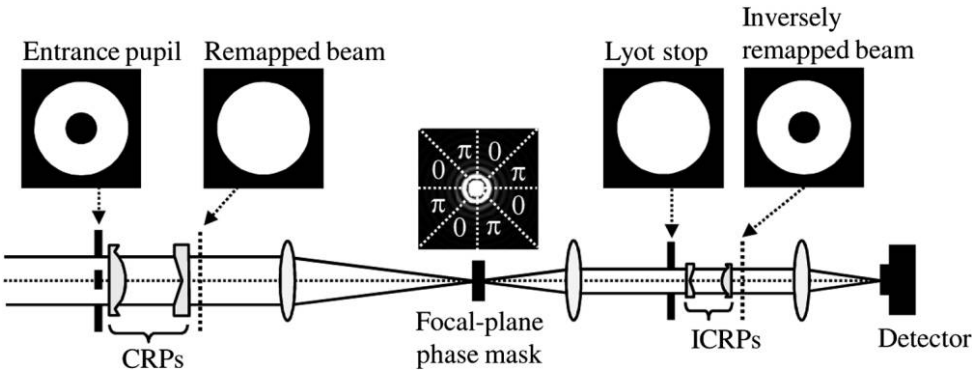


FIG. 3.—Optical configuration of an eight-octant phase-mask coronagraph for a conventional centrally-obscured telescope. The CRPs are used to remove the central obscuration. Reverse correcting devices (inverse CRPs, ICRPs) are also used for improving the field of view.

$$\frac{dz_1}{dr_1} = -\frac{r_1 - r_2(r_1)}{(n/n_0)\sqrt{\{r_1 - r_2(r_1)\}^2 + \{z_2(r_2) - z_1(r_1)\}^2} - \{z_2(r_2) - z_1(r_1)\}}, \tag{4}$$

$$\frac{dz_2}{dr_2} = -\frac{r_1(r_2) - r_2}{(n/n_0)\sqrt{\{r_1(r_2) - r_2\}^2 + \{z_2(r_2) - z_1(r_1)\}^2} - \{z_2(r_2) - z_1(r_1)\}}. \tag{5}$$

Here, n and n_0 are refractive indices of a material of the CRPs and air. The differentiations dz_i/dr_i $(i = 1, 2)$ mean local slopes of the surfaces of the first and second CRPs. These two equations suggest

$$\frac{dz_1}{dr_1} = \frac{dz_2}{dr_2}, \tag{6}$$

which guarantees that the output light beam is collimated if the incoming light beam is collimated.

The functions $z_i(r_i)$ $(i = 1, 2)$, indicating the surface shapes of the CRPs, can be calculated by solving these differential equations. To solve these equations, transfer functions, which describe a relationship between beam radii r_1 and r_2, are required.

Now we design the optical-surface shapes for transforming the centrally-obscured pupil (with a constant intensity $I = 1$) into a clear circular one (with a constant intensity $I = E^2$),

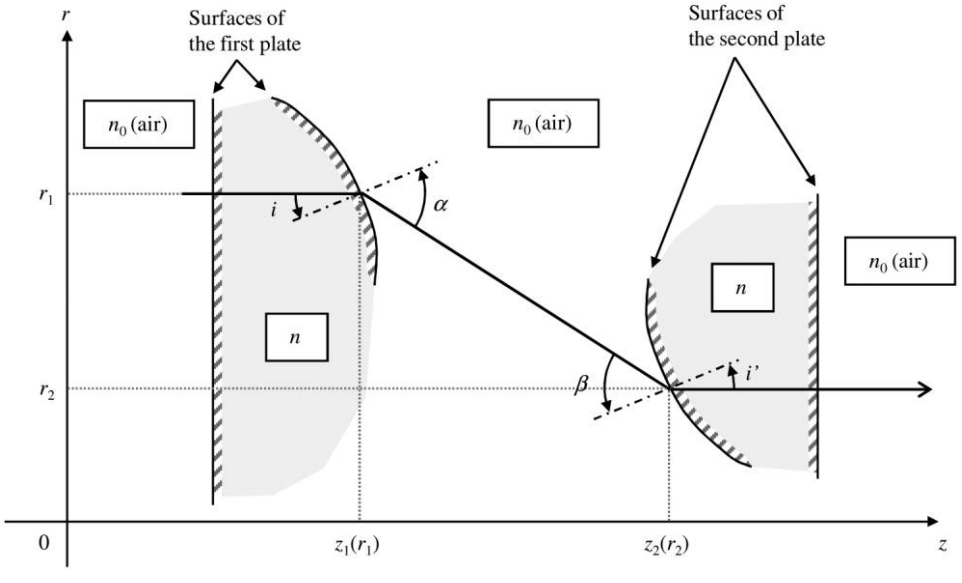


FIG. 4.—A coordinate system for calculating optical surfaces, $z_1(r_1)$ and $z_2(r_2)$, of the CRPs. We followed notation used in Galicher et al. (2005).

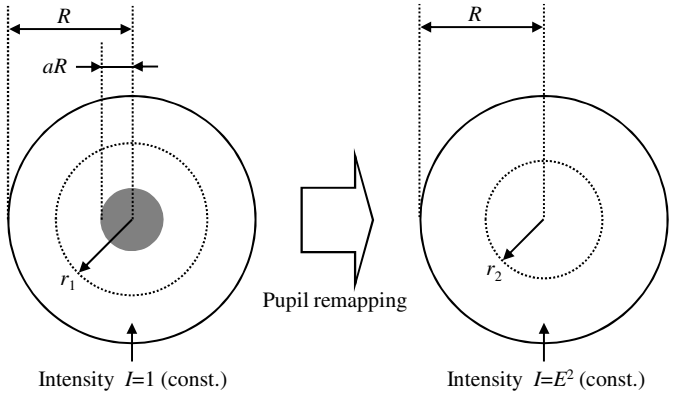


FIG. 5.—Pupil remapping from (*left*) a centrally-obscured pupil to (*right*) a clear circular one.

as shown in Figure 5. In this case, a total intensity inside a circle of a radius r_1 in the input pupil must be identical to that inside a circle of a radius r_2 in the output pupil. Thus, the transfer functions $r_2(r_1)$ and $r_1(r_2)$ can be written as

$$r_2(r_1) = \sqrt{\frac{r_1^2 - (aR)^2}{1 - a^2}}, \tag{7}$$

$$r_1(r_2) = \sqrt{(1 - a^2)r_2^2 + (aR)^2}. \tag{8}$$

In addition, total intensities over the pupil before and after the pupil remapping must be identical. Then E is calculated as

$$E = \sqrt{1 - a^2}. \tag{9}$$

Figure 6 shows the transfer function $r_2(r_1)$ of the CRPs assuming various sizes of the central obscuration ($a = 0.1$, 0.2,0.25 and 0.3).

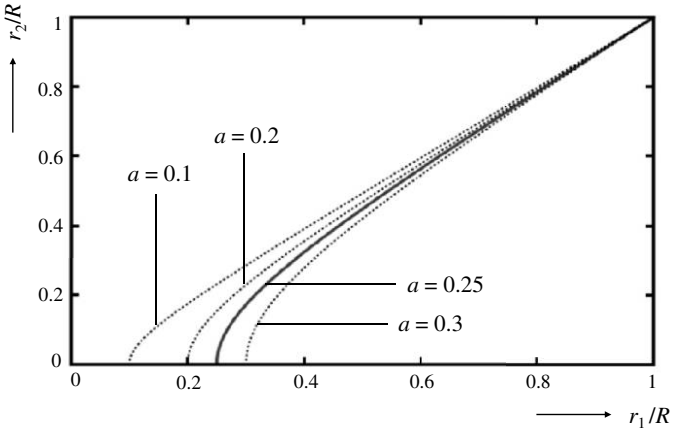


FIG. 6.—The transfer functions of the CRPs for various values of a. The solid line shows the transfer function for manufactured CRPs ($a = 0.25$).

By substituting equations (7) and (8) into equations (4) and (5), we can derive surface shapes $z_1(r_1)$ and $z_2(r_2)$ of the first and second plates. Figure 7 shows the calculated surface shapes numerically derived by using the 4th-order Runge-Kutta method. The surface shapes are described by sag profiles. In this design, we assume a diameter of a pupil $D = 2R = 17.96$ mm, that of a central obscuration $2aR = 4.5$ mm (i.e., $a = 0.25$), and a refractive index $n = 1.425$ (CaF_2 for $\lambda = 1.785$ μm). A separation between the two plates is set to 100 mm. As shown in Figure 7, the first and second plates have convex and concave shapes, respectively.

4. LABORATORY EXPERIMENTS

4.1. Removal of Central Obscuration

We manufactured the designed CRPs shown in Figure 7. Figure 8 shows pictures of the manufactured CRPs. We can see an optical bench through the first plate and a scale through the second plate, which are distorted due to the designed optical-surface shapes. First, we demonstrate that the manufactured CRPs remove a central obscuration. Although the CRPs are designed for H-band observations, laboratory experiments are carried out using a visible laser source (He-Ne laser with a

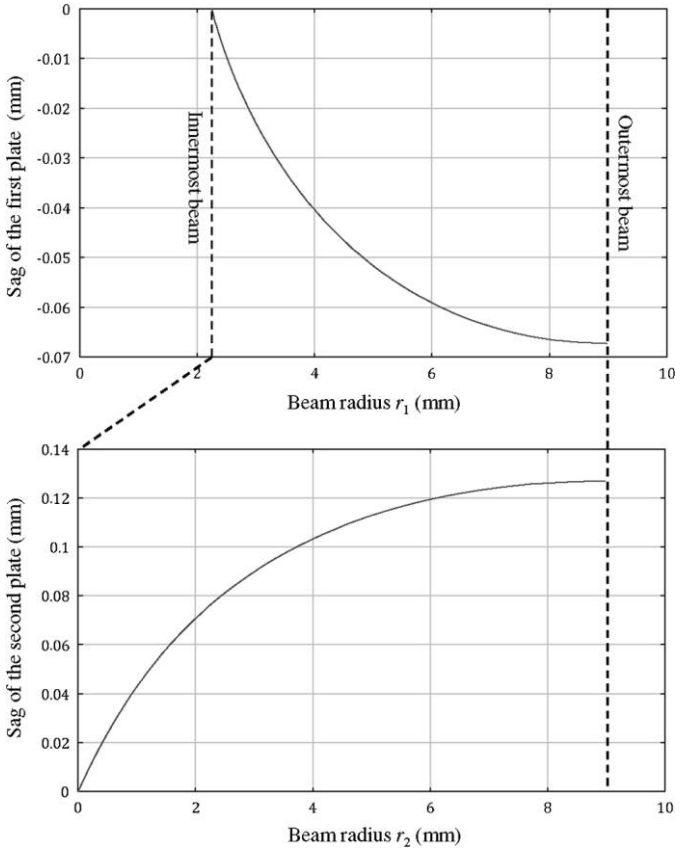


FIG. 7.—Sag profiles of the derived optical-surface shapes of CRPs.

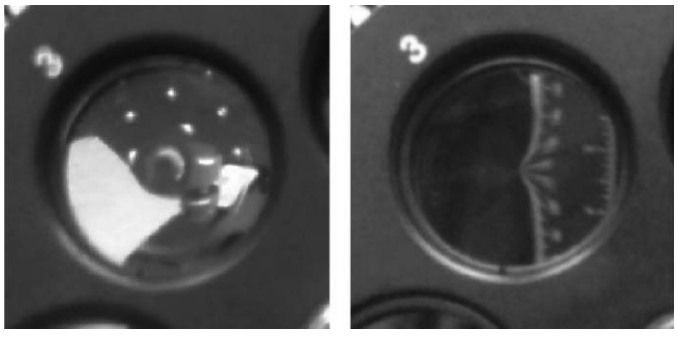


FIG. 8.—Pictures of the manufactured CRPs: (*left*) the first plate and (*right*) the second plate.

wavelength of $\lambda = 0.604$ μm) owing to low-dispersion characteristic of CaF_2.

Figure 9 shows an optical setup for demonstrating the 8OPM coronagraph. The light beam from an optical fiber (He-Ne laser) is collimated by a lens L1, and passes through a centrally-obscured pupil ($D = 17.96$ mm, $aD = 4.5$ mm) that simulates an entrance telescope pupil. The CRPs are placed just behind the obscured pupil to remove the central obscuration. The second plate is mounted on a translating stage to adjust the separation between two plates precisely. The light is then focused by a lens L2 to make a model-star image on a focal plane, where a photonic-crystal 8OPM is placed. The 8OPM is manufactured by photonic-crystal technology (Murakami et al. 2010b). Distances from the centrally-obscured pupil to the lens L2, and from the lens L2 to the focal plane, are both set to 700 mm (a focal length of the lens L2). Thus the pupil and the focal planes are connected by the Fourier transform. Behind a lens L3, a Lyot stop is placed on a relayed pupil plane when we acquire coronagraphic focal-plane images by a lens L4. The relayed pupil plane can also be imaged by replacing the lens L4 with lenses L5 and L6, and moving a CCD camera.

Figure 10 shows (*top*) acquired pupil images and (*bottom*) the intensity profiles without and with the CRPs normalized by total intensities of the images. These pupil images are obtained using the pupil-plane mode (see Fig. 9) without an 8OPM and a Lyot stop. The result demonstrated that the CRPs remove the central obscuration. However, the intensity of light concentrates in the central part of the pupil when the CRPs are used. This central spike-like pattern is possibly due to manufacturing defects of the CRPs, a diffraction effect, misalignment of the optical setup, and so on.

4.2. Combination with an 8OPM Coronagraph

Next, we observed coronagraphic Lyot-stop images by putting the photonic-crystal 8OPM on the focal plane (see Fig. 9). The photonic-crystal 8OPM is optimized at a wavelength of $\lambda = 0.604$ μm. Figure 11 shows observed Lyot-stop images $|E_{p2}(r, \theta)|^2$ without and with the CRPs. We also show numerically-simulated images for comparison. Without the CRPs, the experimental image is similar to the numerically-simulated one. On the other hand, residual light is observed inside the pupil when using the CRPs, although the intensity theoretically becomes zero inside the pupil as demonstrated via the numerical simulation.

Coronagraphic focal-plane images, acquired by using the 8OPM and the Lyot stop, are shown in Figure 12. Coronagraphic focal-plane images without the CRPs are also shown for comparison. A graph shows contrast curves of the acquired images. We calculate the standard deviations $\sigma(\rho)$ of the intensities as a function of the radial distance on the focal plane, normalized by a peak intensity of a PSF obtained by moving the 8OPM to an off-axis position.

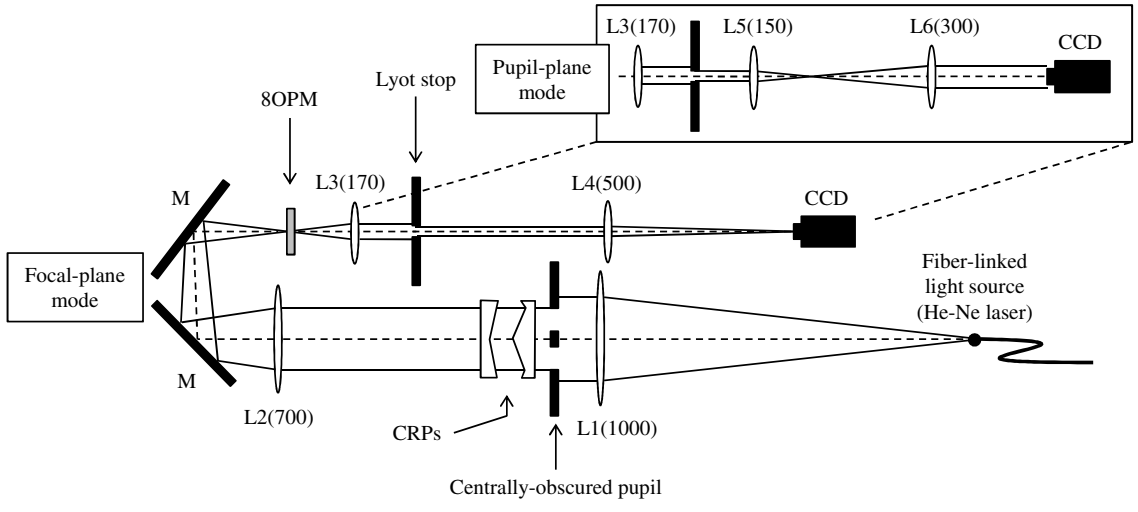


FIG. 9.—The optical setup for demonstrating an eight-octant phase-mask coronagraph with the CRPs. Pupil-plane and focal-plane images can be obtained by switching the imaging modes.

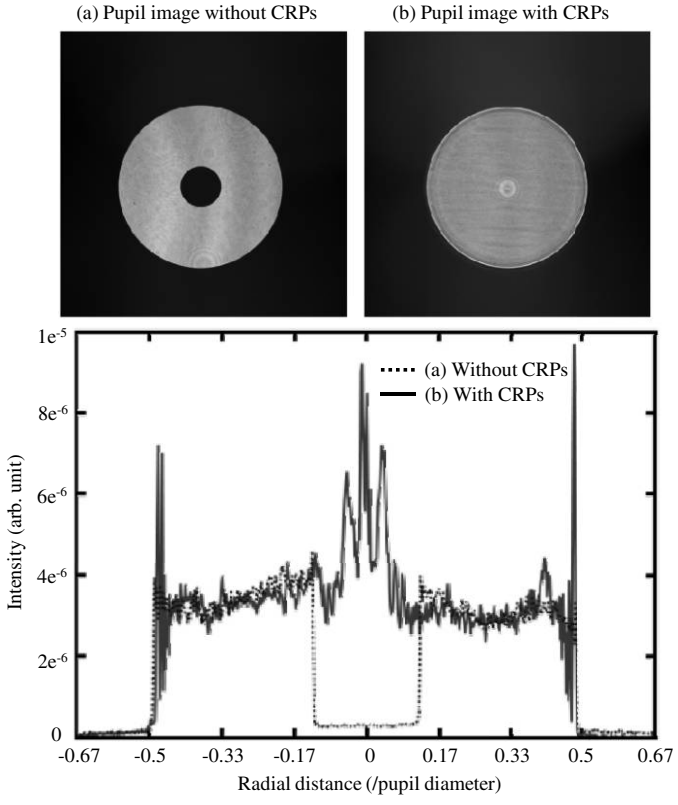


FIG. 10.—Laboratory demonstration of removal of the central obscuration: (*top*) acquired pupil images without and with the CRPs, and (*bottom*) their intensity profiles.

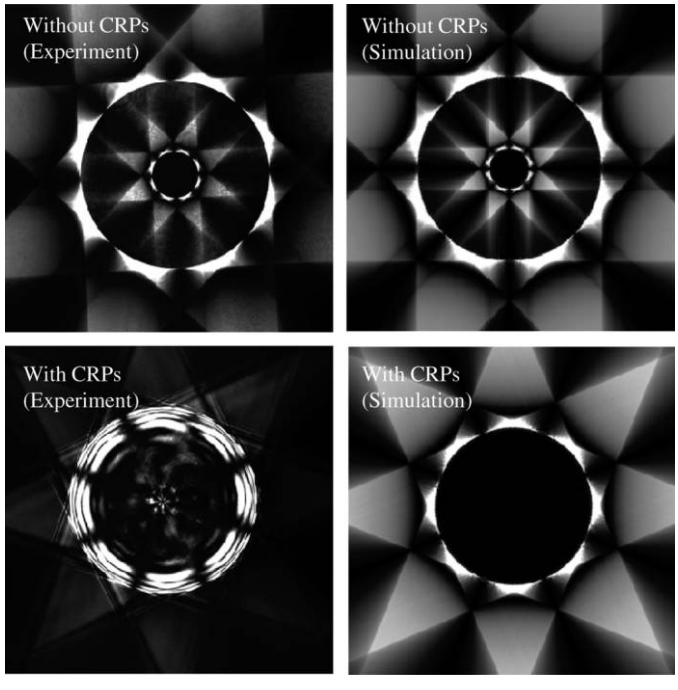


FIG. 11.—Experimental and numerically simulated Lyot-stop images $|E_{p2}(r,\theta)|^2$ without and with the CRP.

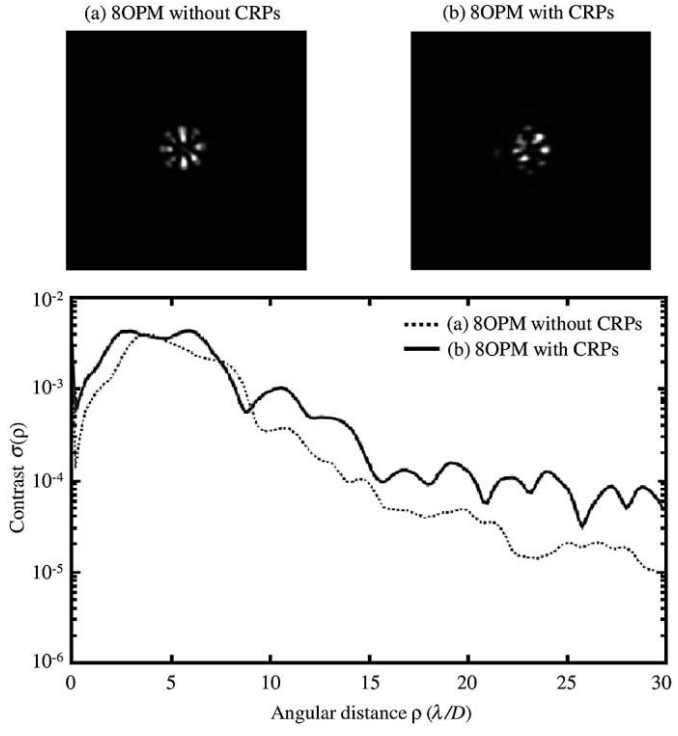


FIG. 12.—Coronagraphic focal-plane images and their contrast curves without and with the CRP.

As shown in Figure 12, the coronagraphic performance is limited to about 4×10^{-3} at peak, and about 10^{-3} at 10 λ/D. We suspect that the coronagraphic performance would be limited by phase aberrations mainly due to the CRPs. In addition, we also expect that an effect of Fresnel diffraction would degrade the achievable contrast. In the next section, we will evaluate, via numerical simulations, these effects on the coronagraphic performance.

4.3. Off-Axis Performance

We also evaluate the performance of off-axis PSFs using the CRPs. Experimental and numerically simulated off-axis PSFs are shown in Figure 13. The first, second, and third columns show the PSFs for off-axis angular separations of 5, 10, and 20 λ/D, respectively. In Figure 13*a*, we show the PSFs obtained in the laboratory experiments. We also show numerically simulated PSFs in Figure 13*b*. As can be seen in Figures 13*a* and 13*b*, the PSFs are severely deteriorated by the CRPs as the off-axis angular separation becomes larger. This means that an effective FOV of the phase-mask coronagraph would be limited.

As mentioned above, one solution for this problem is to recover the quality of the off-axis PSF by putting Inverse CRPs (ICRPs) behind the Lyot-stop to reversely remap the pupil shape. In Figure 13*c*, we show the numerical simulations of coronagraphic focal-plane images using both the CRPs and the

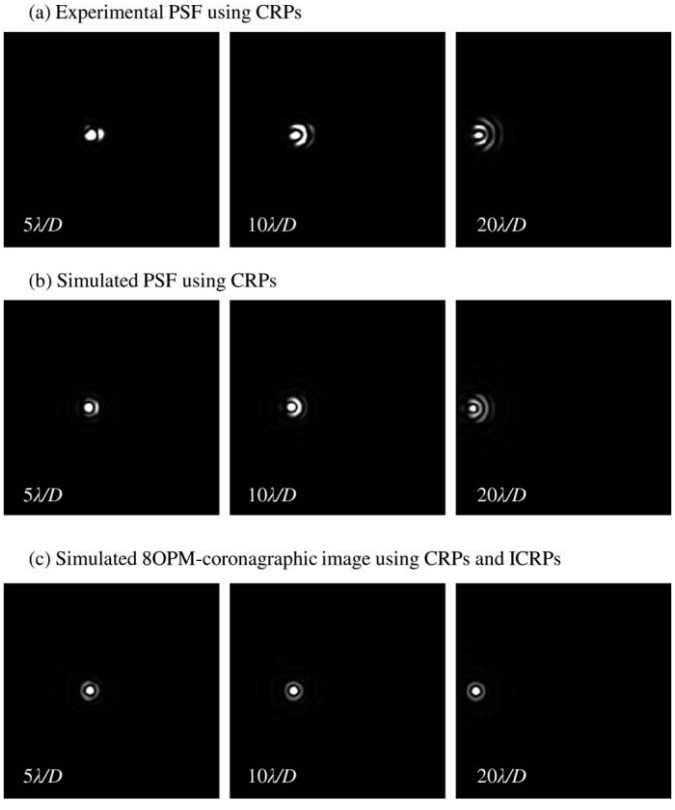


FIG. 13.—Experimental and numerically simulated off-axis PSF images: (*a*) experimental and (*b*) simulated PSFs using CRPs are shown together with (*c*) simulated 8OPM-coronagraphic images using both CRPs and ICRPs.

ICRPs. These numerically simulated images suggest that the effective FOV can be greatly improved.

5. DISCUSSIONS

In our laboratory experiments, the contrast with the CRPs was comparable to that without the CRPs as shown in Figure 12. We suspect that the coronagraphic performance was limited by phase aberrations mainly due to the CRPs, and also by Fresnel diffraction. In this section, we show results of numerical simulations of the 8OPM coronagraph taking into account these effects. In addition, we also discuss chromatic behavior of the manufactured CRPs.

5.1. An Effect of Phase Aberrations

Theoretically, the 8OPM coronagraph realizes perfect rejection of starlight if plane wavefront is incoming to the system. However, phase aberrations of optical components distort the incoming wavefront, and degrade the coronagraphic performance. We carried out numerical simulations of the 8OPM coronagraph taking the phase aberrations of the CRPs into account. First, we generate a centrally-obscured pupil with constant complex amplitude without phase aberrations. Next, random phase aberration, simulating the one due to the first plate, is added to the pupil function. The centrally-obscured pupil is then remapped into a clear circular one, and another random phase aberration, simulating the one due to the second plate, is added. The resultant pupil just behind the second CRP, corresponding to the "remapped beam" in Figure 3, is used as an input of numerical simulations of the 8OPM coronagraph. We assume that the phase aberrations due to the CRPs have power spectra which obey $f^{-2.5}$ power law, where f is a spatial frequency on a pupil plane.

Figure 14 shows results of the numerical simulations. Contrast curves as a function of an angular distance are shown together with the experimentally obtained one (already shown in Fig. 12). The numerical simulations suggest that the phase aberration of each CRP could be roughly $\lambda_V/8.7$ rms at a wavelength $\lambda_V = 0.604$ μm, if the experimentally obtained contrast is limited only by the phase aberrations. It would be important to manufacture CRPs with more precisely polished optical surfaces to improve the coronagraphic performance. Also, it would be necessary to introduce an adaptive optics system for correcting distorted incoming wavefront.

When the phase aberration is $\lambda_V/8.7$ rms in the visible wavelength λ_V, the phase aberration becomes roughly $\lambda_{H0}/24$ rms at the middle wavelength in H band ($\lambda_{H0} = 1.65$ μm), and roughly $\lambda_{Hb}/22$ rms and $\lambda_{Hr}/26$ rms at "blue side" and "red side" of the H band ($\lambda_{Hb} = 1.485$ μm and $\lambda_{Hr} = 1.785$ μm, respectively). Thus, an achievable contrast would become better when the CRPs are used in H band. The graph in Figure 14 also shows simulated contrast curves corresponding to the H band (at

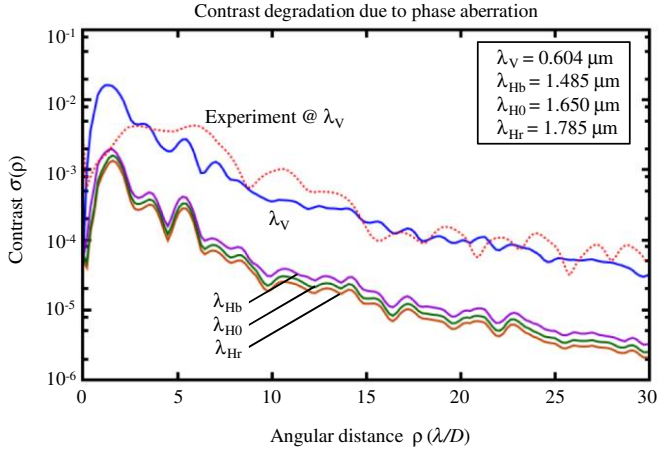


FIG. 14.—Numerical simulations of the 8OPM coronagraph using the CRPs taking phase aberrations into account. A simulated contrast curve assuming the phase aberration of each CRP of about $\lambda_V/8.7$ rms at a wavelength of $\lambda_V = 0.604$ μm is roughly comparable to the experimentally obtained one (*dotted curve*). When the phase aberration is $\lambda_V/8.7$ rms at λ_V, corresponding phase aberration at $\lambda_{Hb} = 1.485$ μm, $\lambda_{H0} = 1.650$ μm, and $\lambda_{Hr} = 1.785$ μm would be about $\lambda_{Hb}/22$, $\lambda_{H0}/24$, and $\lambda_{Hr}/26$ rms, respectively. We also show contrast curves at these three wavelengths in the graph. See the electronic edition of the *PASP* for a color version of this figure.

three wavelengths λ_{Hb}, λ_{H0}, and λ_{Hr}). We can see that the contrast becomes better at longer wavelengths, and the chromatic behavior is small over the whole H-band range (contrast varies within a factor of 3).

5.2. An Effect of Fresnel Diffraction

As described in § 3, the CRPs were designed by using geometric optics. However, an effect of Fresnel diffraction would prevent us from realizing the ideal clear circular pupil. Thus, the effect of the Fresnel diffraction would also degrade the coronagraphic performance.

We carried out numerical simulation of the 8OPM coronagraph taking the Fresnel diffraction into account. First, we generate a space-variant phase of the first CRP, and add it to a centrally-obscured pupil. The space-variant phase introduced by the CRP is written as

$$\phi_{\rm crp}(r,\lambda) = \frac{2\pi(n-1)}{\lambda} Sag(r), \qquad (10)$$

where $Sag(r)$ is an optical-surface shape of the CRP shown in Figure 7. Thin lens approximation is assumed for the CRPs in the numerical simulation. Next, complex amplitude of diffracted light is calculated by the Fresnel-diffraction analysis. Finally, another space-variant phase corresponding to the second CRP is added. The resultant pupil, corresponding to the "remapped beam" in Figure 3, is used as an input of numerical simulations of the 8OPM coronagraph.

Figure 15 shows results of the numerical simulations. Simulated contrast curves are shown together with the experimentally obtained one. To simulate the Fresnel diffraction, we assume the visible wavelength λ_V. It should be noted that the CRPs can be used in visible by slightly shortening a distance between two plates, although they are designed for H band. The numerically-simulated contrast curve at λ_V is much better than that obtained in the laboratory experiment. Thus, it is expected that the Fresnel diffraction would not be a dominant limiting factor.

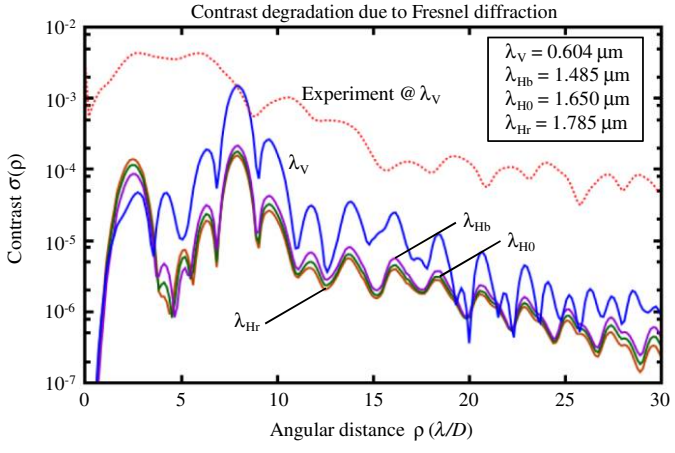


FIG. 15.—Numerical simulations of the 8OPM coronagraph using the CRPs taking Fresnel diffraction into account. Simulated contrast curves assuming the Fresnel diffraction at wavelengths $\lambda_V = 0.604$ μm, $\lambda_{Hb} = 1.485$ μm, $\lambda_{H0} = 1.650$ μm, and $\lambda_{Hr} = 1.785$ μm are shown together with the experimentally obtained one (*dotted curve*). See the electronic edition of the *PASP* for a color version of this figure.

We also carried out numerical simulations of the Fresnel diffraction at three wavelengths in H band (λ_{H0}, λ_{Hr}, and λ_{Hb}). The coronagraphic performance becomes better in H band than that obtained in visible, but the contrast is still severely limited (a peak contrast is about 10^{-4}). For better coronagraphic performance, it would be necessary to optimize designs of the CRPs taking the Fresnel diffraction into account. It might also be interesting to use an additional apodizer behind the second CRP to generate a clear circular aperture with constant amplitude and phase. We can see that the chromatic behavior due to the Fresnel diffraction also seems to be small over the whole H-band range (contrast varies roughly within a factor of 2).

Finally, it should be noted that the numerical simulations shown in this section are still preliminary. Further investigations are necessary for fully understanding these effects, and for improving the coronagraphic performance.

6. CONCLUSION

We proposed the pupil-remapping plates, called the central-obscuration removal plates (CRPs), to remove shade of a secondary mirror. It is expected that the CRPs will maximize the performance of phase-mask coronagraphs installed into conventional centrally-obscured telescopes in future.

We carried out the laboratory demonstration of the manufactured CRPs made of CaF_2, and confirmed that the CRPs remove the central obscuration. We also evaluated the coronagraphic performance of an eight-octant phase-mask coronagraph combined with the CRPs. As a result, the achieved contrast with the CRPs was comparable to that without the CRPs. We suspect that the contrast would be limited by the phase aberrations due to the CRPs, and by the effect of the Fresnel diffraction. We carried out numerical simulations of the 8OPM coronagraph taking these effects into account. The numerical simulations suggest that the current coronagraphic performance in the laboratory experiments could be limited mainly by the phase aberrations. The numerical simulations also suggest that the effects of the chromatic behavior due to the phase aberrations and the Fresnel diffraction could be small over the whole wavelength range in H band. We expect that the coronagraphic performance would be improved by the CRPs with more precisely polished optical surfaces, and by an adaptive optics system, to reduce the phase aberrations. In addition, appropriate design of the CRPs taking the Fresnel diffraction into account will be one of our interesting future works.

We thank Nemanja Jovanovic and Garima Singh of the National Astronomical Observatory of Japan (NAOJ) for valuable discussions and support for the experiments on the CRPs. We

are grateful to Moritsugu Sakamoto and Kazuhiko Oka of Hokkaido University for their helpful comments on numerical simulations of Fresnel diffaction. This research was partly supported by the NAOJ, and by the Japan Society for the Promotion of Science (JSPS) through KAKENHI (23740139, 24103501, and 25610038).

REFERENCES

Abe, L., Murakami, N., Nishikawa, J., & Tamura, M. 2006, A&A, 451, 363
Absil, O., Milli, J., Mawet, D., Lagrange, A.-M., Girard, J., Chauvin, G., Boccaletti, A., Delacroix, C., et al. 2013, A&A, 559, L 12
Beuzit, J.-L., Feldt, M., Dohlen, K., Mouillet, D., Puget, P., Wildi, F., Abe, L., Antichi, J., et al. 2008, Proc. SPIE, 7014, 701418
Boccaletti, A., Abe, L., Baudrand, J., Daban, J.-B., Douet, R., Guerri, G., Robbe-Dubois, S., Bendjoya, P., et al. 2008, Proc. SPIE, 7015, 70151 B
Foo, G., Palacios, D. M., & Swartzlander, G. A.Jr. 2005, Opt. Lett., 30, 3308
Galicher, R., Guyon, O., Otsubo, M., Suto, H., & Ridgway, S. 2005, PASP, 117, 411
Guyon, O. 2003, A&A, 404, 379
Kalas, P., Graham, J. R., Chiang, E., Fitzgerald, M. P., Clampin, M., Kite, E. S., Stapelfeldt, K., Marois, C., et al. 2008, Science, 322 1345
Kuzuhara, M., Tamura, M., Kudo, T., Janson, M., Kandori, R., Brandt, T. D., Thalmann, C., Spiegel, D., et al. 2013, ApJ, 774, 11
Lagrange, A.-M., Gratadour, D., Chauvin, G., Fusco, T., Ehrenreich, D., Mouillet, D., Rousset, G., Rouan, D., et al. 2009, A&A, 493, L 21
Lozi, J., Martinache, F., & Guyon, O. 2009, PASP, 121, 1232
Macintosh, B. A., Graham, J. R., Palmer, D. W., Doyon, R., Dunn, J., Gavel, D. T., Larkin, J., Oppenheimer, B., et al. 2008, Proc. SPIE, 7015, 701518
Marois, C., Macintosh, B., Barman, T., Zuckerman, B., Song, I., Patience, J., Lafrenière, D., & Doyon, R. 2008, Science, 322, 1348
Martinache, F., & Guyon, O. 2009, Proc. SPIE, 7440, 74400 O
Mawet, D., Pueyo, L., Carlotti, A., Mennesson, B., Serabyn, E., & Wallace, J. K. 2013, ApJS, 209, 7
Mawet, D., Riaud, P., Absil, O., & Surdej, J. 2005, ApJ, 633, 1191
Mawet, D., Riaud, P., Baudrand, J., Baudoz, P., Boccaletti, A., Dupuis, O., & Rouan, D. 2006, A&A, 448, 801
Mawet, D., Serabyn, E., Liewer, K., Burruss, R., Hickey, J., & Shemo, D. 2010, ApJ, 709, 53
Mawet, D., Serabyn, E., Stapelfeldt, K., & Crepp, J. 2009, ApJ, 702, L 47
Mawet, D., Serabyn, E., Wallace, J.K., & Pueyo, L. 2011, Opt. Lett., 36, 1506
Murakami, N., & Baba, N. 2005, PASP, 117, 295
Murakami, N., Guyon, O., Martinache, F., Matsuo, T., Yokochi, K., Nishikawa, J., Tamura, M., Kurokawa, T., et al. 2010, Proc. SPIE, 7735, 773533
Murakami, N., Nishikawa, J., Yokochi, Tamura, M., Baba, N., & Abe, L. 2010, ApJ, 714, 772
Murakami, N., Uemura, R., Baba, N., Nishikawa, J., Tamura, M., Hashimoto, N., & Abe, L. 2008, PASP, 120, 1112
Pueyo, L., & Norman, C. 2013, ApJ, 769, 102
Rouan, D., Riaud, P., Boccaletti, A., Clénet, Y., & Labeyrie, A. 2000, PASP, 112, 1479
Serabyn, E., Mawet, D., & Burruss, R. 2010, Nature, 464, 1018
Serabyn, E., Mawet, D., Bloemhof, E., Haguenauer, P., Mennesson, B., Wallace, K., & Hickey, J. 2009, ApJ, 696, 40
Soummer, R., Aime, C., & Falloon, P. E. 2003, A&A, 397, 1161
Thalmann, C., Carson, J., Janson, M., Goto, M., McElwain, M., Egner, S., Feldt, M., Hashimoto, J., et al. 2009, ApJ, 707, L 123